SLAC-PUB-11467
9/07/2005

Study of the low momentum compaction B-factory*

S. Heifets, A. Novokhatski
Stanford Linear Accelerator Center, Stanford University, Stanford, CA 94309, USA

Abstract

For a given rf frequency, the quasi-isochronous lattice allows, in principle, to double the number of bunches compared with the nominal lattice. We explore such a possibility considering the beam stability and luminosity of the PEP-II B-factory.

1 Introduction

The high luminosity is achieved in the PEP-II B-factory by filling each other RF bucket. The luminosity might be increased further by increasing the bunch current. However, the maximum bunch current is limited mostly by the beam-beam effect. There are several other effects limiting the bunch current such as loading of the feedback system and the bunch lengthening (approximately $\Delta\sigma = 1$ mm per mA of the bunch current). Distortion of the Gaussian longitudinal bunch profile increases heating due to the widening bunch spectrum and may limit the bunch current. The microwave instability and the head-tail effect may be important although, at the present for PEP-II, the bunch current threshold of the microwave instability is more than 15 mA, approximately 7 times higher than actual bunch current.

One way to increase luminosity for a given bunch current and rf frequency is to fill each rf bucket. However, the parasitic crossings, the bunch-by-bunch feedback system, and limited rf power may prevent us to go in this direction.

In this paper we want to explore another approach: doubling of the number of bunches per rf wave length. That can be achieved, in principal, using the quasi-isochronous lattice with low momentum compaction factor α.

There are many questions to be answered whether such approach can be used to increase luminosity. Here we address only few of them: the lattice design, the equilibrium

*Work supported by Department of Energy contract DE–AC02–76SF00515

bunch profile and the bunch lengthening, the issue of the parasitic crossings, the rf stability, the microwave and the longitudinal head-tail instabilities. Other questions such as transverse head-tail instabilities might be addressed later. Such problems as parasitic crossings and limited rf power are the same as for the fill of each rf bucket but the longitudinal head-tail instability looks like the main objection to the approach. If these problems can be solved, then in ideal case, filling each bucket and using quasi-isochronous lattice, the number of bunches could be increased by a factor of four.

In the next section we consider dependence of the luminosity and beam-beam parameter on the momentum compaction factor.

2 Dependence of the luminosity on α

The luminosity is proportional to the overlapping of the distribution functions of colliding bunches. The later depends on the zero-current rms bunch length σ_0 and on the bunch profile. For equal bunch currents $I_B = eN_B f0$, transverse rms $\sigma^*_{x,y}$, and β^*_y function at the interaction point (IP) for both beams,

$$
\begin{aligned}
&L = L_0 J_L(\frac{\sigma_0}{\beta^*_y}), \quad L_0 = \frac{N_B^2 f_0}{4\pi\sigma^*_x\sigma^*_y}, \\
&J_L(p) = 2\int \frac{dsdz f_1(z+s-\Delta s/2) f_2(z-s+\Delta s/2)}{\sqrt{1+p^2(s/\sigma_0)^2}}. \qquad (1)
\end{aligned}
$$

Here $f(z)$ is the longitudinal distribution function normalized as $\int f(z)dz = 1$, z is the distance of a particle from the bunch center, $z > 0$ is for a particle shifted in the direction of the propagation of the beam. The longitudinal position of a particle in two bunches is $s_{1,2} = \pm(ct + z) + \Delta s/2$ where $\Delta s/2$ is the longitudinal offset equal to the distance of the bunch centroids of the colliding bunches from the waist of the β-function (i.e. from the interaction point). The form factor J_L describes the hour-glass effect: reduction of the luminosity L from the nominal L_0.

It is convenient to express the luminosity in terms of the beam-beam parameter ξ_{BB} considering the maximum value of the later as fixed experimental parameter. If ξ_{BB} is defined as the tune shift averaged over the bunch interacting with the opposite beam, then it also depends on the shape of the distribution function.

$$
\begin{aligned}
&\xi_{BB} = \xi^0_{BB} J_\xi(\frac{\sigma_0}{\beta^*_y}), \quad \xi^0_{BB} = \frac{N_B r_e \beta^*_y}{2\pi\gamma\sigma^*_x\sigma^*_y}, \\
&J_\xi(p) = 2\int dsdz f_1(z+s-\Delta s/2) f_2(z-s+\Delta s/2)\sqrt{1+p^2(s/\sigma_0)^2}. \qquad (2)
\end{aligned}
$$

The ξ_{BB} defined in this way should be used for estimates of the achievable luminosity in the upgrade of the B-factory rather than ξ^0_{BB}. In this case, given the bunch population N_B and the beam-beam parameter ξ_{BB}, the hour-glass effect is given by the ratio $(1/\beta_y^*)(J_L/J_\xi)$,

$$L = \frac{\gamma N_B f_0}{2r_e}\,\xi_{BB}\beta_y^*\,\frac{J_L(\sigma_0/\beta_y^*)}{J_\xi(\sigma_0/\beta_y^*)}. \tag{3}$$

The hour-glass form-factors J_L and J_ξ for Gaussian bunches are shown in Fig. (1). The ratio J_L/J_ξ is equal to one at $\sigma_0/\beta_y^* = 0$ and drops to 0.716 at $\sigma_0/\beta_y^* = 1$.

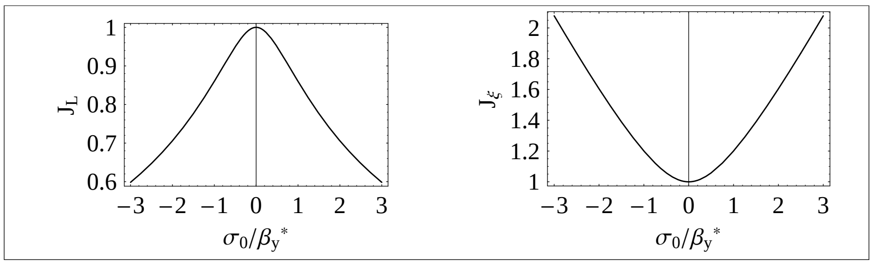

Figure 1: The form-factors J_L and J_ξ for Gaussian bunches.

The hour-glass form factor (J_L/J_ξ) depends on the momentum compaction factor α. For a fixed rf voltage V_{rf}, the argument σ_0/β_y^* is proportional to $(1/\beta_y^*)\sqrt{\alpha}$. Hence, in the zero approximation, the hour-glass form factor does not change if β_y^* varies proportional to $\sqrt{\alpha}$. Then, reducing α and scaling $\beta_y^* \propto \sqrt{\alpha}$ one can increase the luminosity $L \propto (1/\sqrt{\alpha})$. Such argument, however, ignores the distortion of the bunch profile due to potential well distortion (PWD). We return to the effect of the PWD below after discussion of the longitudinal dynamics with small α in the next two sections and then discuss other implications of the low α. Here we want to mention that, eventually, the onset of the longitudinal head-tail instability sets the limit on the minimal α.

3 Longitudinal dynamics with small α

As it is well known [1], the longitudinal dynamics is described by the equations

$$\begin{aligned}\frac{dz}{dt} &= -c\delta(\alpha_0 + \alpha_1\delta)\delta,\\ \frac{d\delta}{dt} &= \frac{eV\omega_0}{2\pi E_0}\cos(\phi_s - \frac{\omega_{rf}z}{c}) - \frac{\omega_0 U}{2\pi E_0},\end{aligned} \tag{4}$$

where z is the shift of a particle from the bunch centroid ($z > 0$ is shift toward the head of the bunch), $\delta = (E - E_0)/E_0$ is the energy deviation, and c is the velocity of light. Other parameters are: ω_0 is the revolution frequency, ϕ_s is the rf phase, $\cos\phi_s = U/E_0$,

$\alpha = \alpha_0 + \delta\alpha_1$ is the momentum compaction, E is the beam energy, V and U are the rf voltage and the energy loss (including wake field) per turn, respectively.

Eq. (4) shows that there are two stable fixed points (FP):

$$\{(1).\quad \frac{\omega_{rf} z_1}{c} = 0, \delta_1 = 0\}, \quad \{(2).\quad \frac{\omega_{rf} z_2}{c} = 2\phi_s, \delta_2 = -\frac{\alpha_0}{\alpha_1}\}. \tag{5}$$

The motion in the small vicinity of the fixed points is stable (provided the phase $0 < \phi_s < \pi/2$) with the same synchrotron frequency Ω_s proportional to α_0,

$$\Omega_s^2 = \frac{eV\alpha_0\omega_0\omega_{rf}}{2\pi E_0}\sin\phi_s. \tag{6}$$

Hence, generally, there are two bunches within the rf wave length centered at the two FPs. The second bunch (centered at the 2nd FP) moves ahead of the 1st bunch (centered at the 1st FP) and, in the region with the dispersion D_x, is shifted horizontally by $\Delta x = -\frac{\alpha_0}{\alpha_1}D_x$ relative to the centroid of the first bunch. For the nominal lattice, where α_0/α_1 is large, the shift is larger than the beam pipe aperture, and the phase plane looks like the upper plot in Fig. 2. For sufficiently small α_0, the second stable point may be within the physical aperture and two bunches can be stable within one rf wave length.

The ratio α_0/α_1 defines not only the energy shift of the bunches but also the energy acceptance for each bunch. It has to be large compared to the rms energy spread δ_0, say, $\alpha_0/\alpha_1 >\simeq 10\delta_0$. Parameter α_1 is given, mostly, by sextupoles and, as in the example below, $\alpha_1 \simeq 0.05$. Therefore, the lattice has to be designed to give small but not too small α_0, only by an order of magnitude smaller than the nominal $\alpha_0 = 2.4E-3$.

Fortunately, PEP-II HER electron ring has quite small $\delta_0 = 6.1E-4$, Another specific advantage of the PEP-II is that it operates using the high repetition rate of injection what relaxes requirements for the dynamic aperture and the energy acceptance.

4 Lattice design

The lattice for quasi-isochronous ring was designed before [2]. Here we reproduce the design for the arcs ignoring the straight sections and matching sections. In this case, the ring comprises 6 arcs, each arc has 4 super-cells. Each 45.6 m long super-cell is, basically, 3 unequal FODO cells and have mirror symmetry around the super-cell center. There are six bend dipoles per super-cell. Bends are the same as in the present nominal design, each with the length 5.4 m and the bend angle $2\pi/144$ radian. The phase advance per super-cell is $\mu_x/2\pi = 0.75$ and $\mu_y/2\pi = 0.25$. Maximum $\beta_{x/y} = 38.8/76.9$ m, maximum $D_x = 1.85$ m. The first quadrupole is the strongest, $B'_y \simeq 15.1\ T/m$. Sensitivity to the field errors can be seen from variation of α_0 with the parameter $K_1 = B'/(B\rho)$ of the first quadrupole, $d\alpha_0/dK_1 \simeq 0.006\ m^2$. The super-cell includes the chromatic sextupoles. Parameters of the super-cell are given in the Appendix in the MAD format. The optics is shown in Fig. (3).

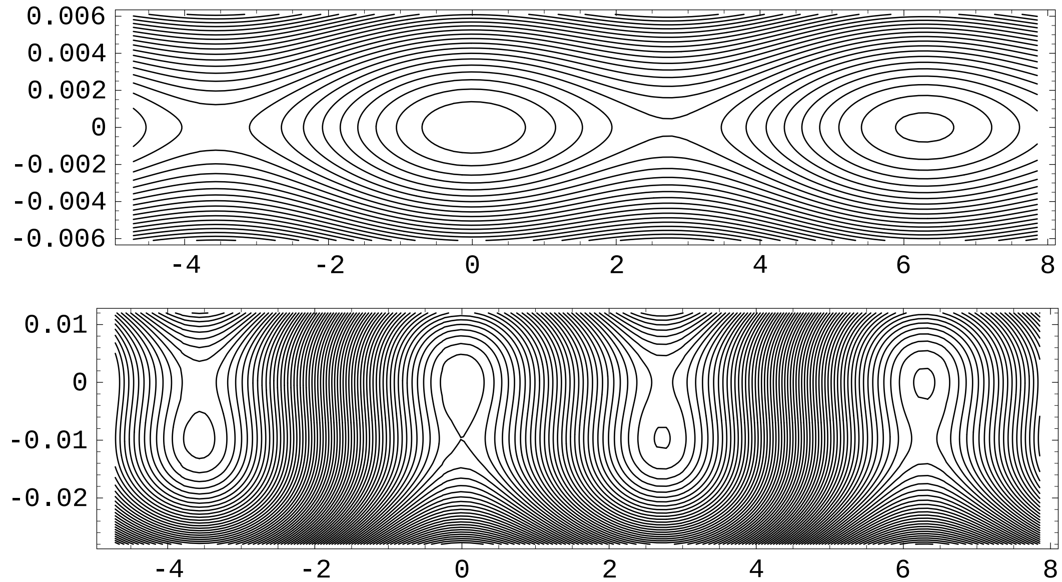

Figure 2: Phase plot for the Hamiltonian $H(\delta,\zeta) = \alpha_0\delta^2/2 + \alpha_1\delta^3/3 - \lambda(\sin[\phi-\zeta] - \sin[\phi]) - \lambda\zeta\cos[\phi]$. Parameters are $\lambda = 2.0E-7$, $\alpha_1 = 5.5E-2$, and $\alpha_0 = 5.0E-2$ (above), and $\alpha_0 = 5.34E-4$ (bottom). Note the different vertical scale for two plots.

Momentum compaction calculated with MAD is

$$\alpha = 5.34410^{-4} + 0.05542\delta - 0.0662\delta^2, \tag{7}$$

Hence, $\alpha_0 = 5.344E-4$, $\alpha_1 = 0.0554$, and the energy separation of the stable points α_0/α_1 corresponds to $15.81\delta_0$, and the offset $\Delta x = 1.78$ cm. Note that α_0 is smaller than the nominal $\alpha_0 = 2.7E-3$ only by a factor of five.

The same lattice can be used to make the lattice isochronous. Fig. (4) shows the lattice parameters for negative $\alpha_0 = -1.03E-4$. The lattice is the same but the strength of the first quadrupole increased to $K_1 = 0.505\ m^{-2}$ from $K_1 = 0.49\ m^{-2}$ for $\alpha_0 = 5.344E-4$.

The design of the lattice for the LER positron ring can be different and based on the lattice with missing bends. The ratio α_0/α_1 in both rings has to be the same to have collisions. We also assume the zero dispersion at the interaction point (IP).

5 Bunch profile

The equilibrium steady-state longitudinal bunch profile is given by the Haissinski solution. For $\phi_s \simeq \pi/2$, the FPs are well separated, $\Delta z \simeq \lambda_{rf}/2$. For realistic bunches $\sigma_l << \Delta z$,

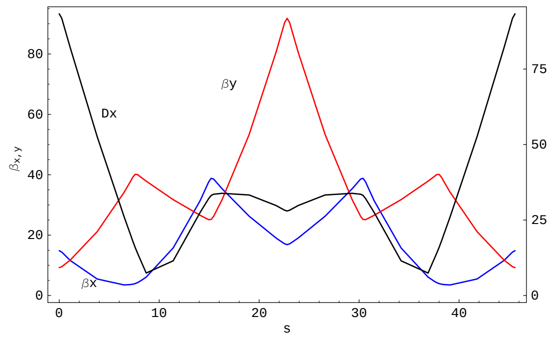

Figure 3: Twiss parameters for the quasi-isochronous lattice with $\alpha_0 = 5.344E-4$.

and the bunch profile $\rho(z)$ can be written as the sum of distributions for two bunches. The bunch profile for the second (leading) bunch is

$$f_2(z) = \frac{1}{N_2} e^{-\frac{(z-z_2)^2}{2\sigma_0^2} + \Lambda \int_z^\infty dz' f_2(z') S(z'-z)}. \tag{8}$$

Here $S(z)$ is given by the longitudinal wake $W^\delta(z)$, $S(z) = \int_0^z W^\delta(z')dz'$, $S(z) = 0$ for $z < 0$, and

$$\Lambda = \frac{N_b r_e}{2\pi R \gamma \alpha_0 \delta_0^2}, \tag{9}$$

where r_e is the classical electron radius, γ is relativistic factor, and δ_0 is the rms relative energy spread.

The bunch profile for the first bunch has to take into account the wake generated by the second bunch

$$f_1(z) = \frac{1}{N_1} e^{-\frac{z^2}{2\sigma_0^2} - \Lambda \int_z^\infty dz' f_1(z') S(z'-z) - \Lambda \int dz' f_2(z') S(z'-z)}. \tag{10}$$

The normalization constants $N_{1,2}$ are given by the condition $\int f_{1,2}(z)dz = 1$. The energy spread is defined by the synchrotron radiation and is equal for both bunches. Therefore, parameters σ_0 and Λ are the same as for the leading bunch. Because f_2 is large only for $z \simeq z_2$, The last term in Eq. (10) gives mostly the current dependent shift of the distribution $f_1(z)$,

$$\int_z^\infty dz' f_2(z') S(z'-z) = -zW^\delta(z_2) + const \tag{11}$$

.

However, because the broad-band wake at large $z_2 >> \sigma_0$ is small, the shift can be neglected. For the well separated bunches, the quantum diffusion between bunches is exponentially small.

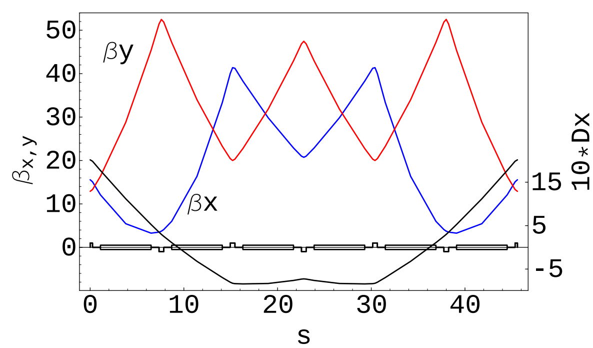

Figure 4: Twiss parameters for the quasi-isochronous lattice with $\alpha_0 = -1.0\,10^{-4}$.

Eq. (8) shows that the bunch profile depends only on two parameters: Λ and the zero current rms bunch length σ_0. Both parameters depend on α, $\Lambda \propto 1/\alpha$ and $\sigma_0 = c\alpha_0\delta_0/\Omega_s \propto \sqrt{\alpha_0/V_{rf}}$. It should be noted that σ_0 depends on the rf voltage V_{rf}. Therefore, variation of α_0 at the constant σ_0 implies simultaneous variation of the rf voltage.

Note that the wake term enters in Eq. 8, 10 with the opposite sign. Therefore, the dynamics of the leading bunch is the same as the dynamics of a bunch in the lattice with the negative momentum compaction factor.

6 The longitudinal Wake

At small z, the wake $W^\delta(z) \propto z$, and $S(z) \propto z^2 \simeq \sigma^2 \propto \alpha_0$ and the current dependent term may be constant with α_0[†]. In this case, one can expect that the contribution of the wake decreases with α_0 and the bunch lengthening is limited. Unfortunately, that does not happened for more realistic wake fields and rms bunches.

We model the wake field of a point-like bunch for the LER PEP-II B-factory adding contributions of the experimentally measured modes of six RF cavities, resistive wall, and the inductive components of the ring. The later are described by the inductive-like model with the wake W^δ_L,

$$W^\delta_L(z) = \frac{L}{\sqrt{\pi z a^3}}(1 - \frac{z}{a})e^{-\frac{z}{a}}, \tag{12}$$

where the inductance $L = 80$ nH corresponds to the estimated inductance of the ring

[†]This comment belongs to C. Pellegrini

and the parameter $a = 0.285$ cm is chosen to reproduce the total loss factor of the small vacuum components of the ring.

In the study described below we use the wake $W(z)$ convoluted with the Gaussian bunch with rms $\sigma_0 = 8$ mm. The wake $W(z)$ is shown in Fig. (5).

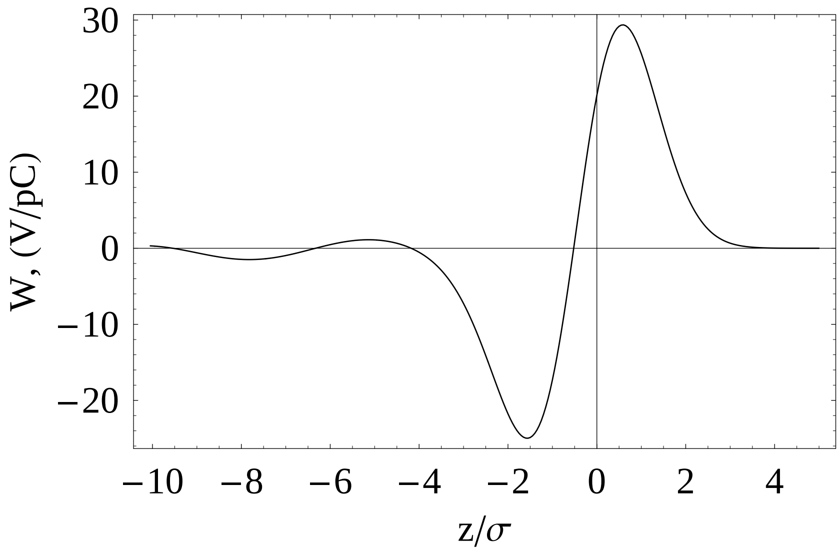

Figure 5: Wake field obtained by convolution of the $W\delta(z)$ with the $\sigma = 8$ mm Gaussian distribution.

7 Effect of the PWD on luminosity

The potential well distortion (PWD) makes the first (leading) bunch shorter and the second (trailing) bunch longer. Example of the bunch profile with such a wake for low α is shown in Fig. (6). The trailing bunch has the usual tilt forward while the leading bunch tilt backward and has smaller rms due to the negative sign of the wake term in Eq. 8. The wake field and parameters used in calculations are taken for the impedance model and PEP-II parameters.

Quantitatively, the effect of the PWD depends on the sign of the momentum compaction α_0 and is quite different for the leading and trailing bunches, see Fig. (7).

Both the bunch lengthening (shortening) and the tilt of the bunch profile affect the luminosity. Variation of the hour-glass form-factors J_L and J_ξ with the momentum compaction α_0 taking into account the PWD has been calculated varying $\sigma_0 \propto \sqrt{\alpha_0}$ (for fixed V_{rf}), scaling the Haissinski parameter $\Lambda \propto (1/\alpha_0)$, and $\beta_y^* \propto \sqrt{\alpha_0}$. Variation of the form factors J_L and J_ξ with α_0 in this case is only due to PWD distortion of the distribution

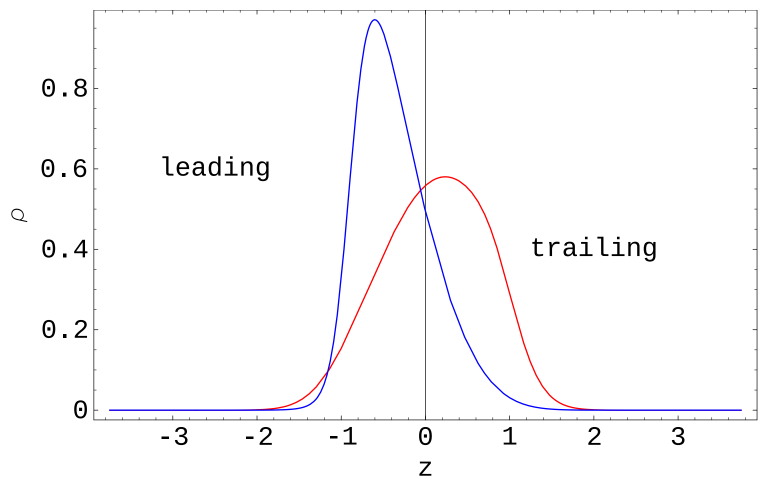

Figure 6: An example of the bunch profiles for the leading (the bunch centered at the 2nd FP, blue line) and trailing bunch(centered at the 1st FP, red line). Parameter $\alpha_0 = 0.8\,10-3$. The zero current $\sigma_0 = 1$ cm, the bunch current $I_B = 2.5$ mA.

functions. It is worth to remind that the luminosity $L \propto (1/\sqrt{\alpha})\,(J_L/J_\xi)$ and grows as $(1/\sqrt{\alpha})$ for small α for constant (J_L/J_ξ). Result of calculations are shown in Fig. 8.

8 Parasitic crossings

One of the main problem with the large number of bunches is caused by the parasitic crossings. The problem is essential for the fill with bunches in the every rf bucket even for the nominal lattice. The doubling of the bunch number in the quasi-isochronous lattice encounters the same problem. However, in the later case there are two type of parasitic crossings. If each rf bucket is filled with two bunches in the quasi-isochronous lattice, the parasitic crossings take place at the distances $\simeq n\lambda_{rf}/4$, where n is an integer and $n = 0$ corresponds the IP collision. For PEP-II B-factory, $\lambda_{rf} = 60$ cm and collisions with $n = \pm 1$ and $n = \pm 2$ take place at the distances 15 cm and 30 cm from IP, before beams are separated in the B1 magnet. Therefore, the beam-beam tune shifts caused by the symmetric parasitic crossings on both sides of the IP tune would cancel each other due to the phase advance $\simeq \pi$ between such collisions. The next parasitic crossings take place at the distances $\pm 3\lambda/4$ and $\pm\lambda$. The last are the same as the parasitic crossings for the present fill of each other rf bucket. Hence, the only new additional parasitic crossings are the interaction at $\pm 3\lambda/4 = 45$ cm inside of the B1 magnet. Hopefully, reduction of the luminosity due to such a crossing is less than the gain due to double number of bunches per ring although this question needs more study.

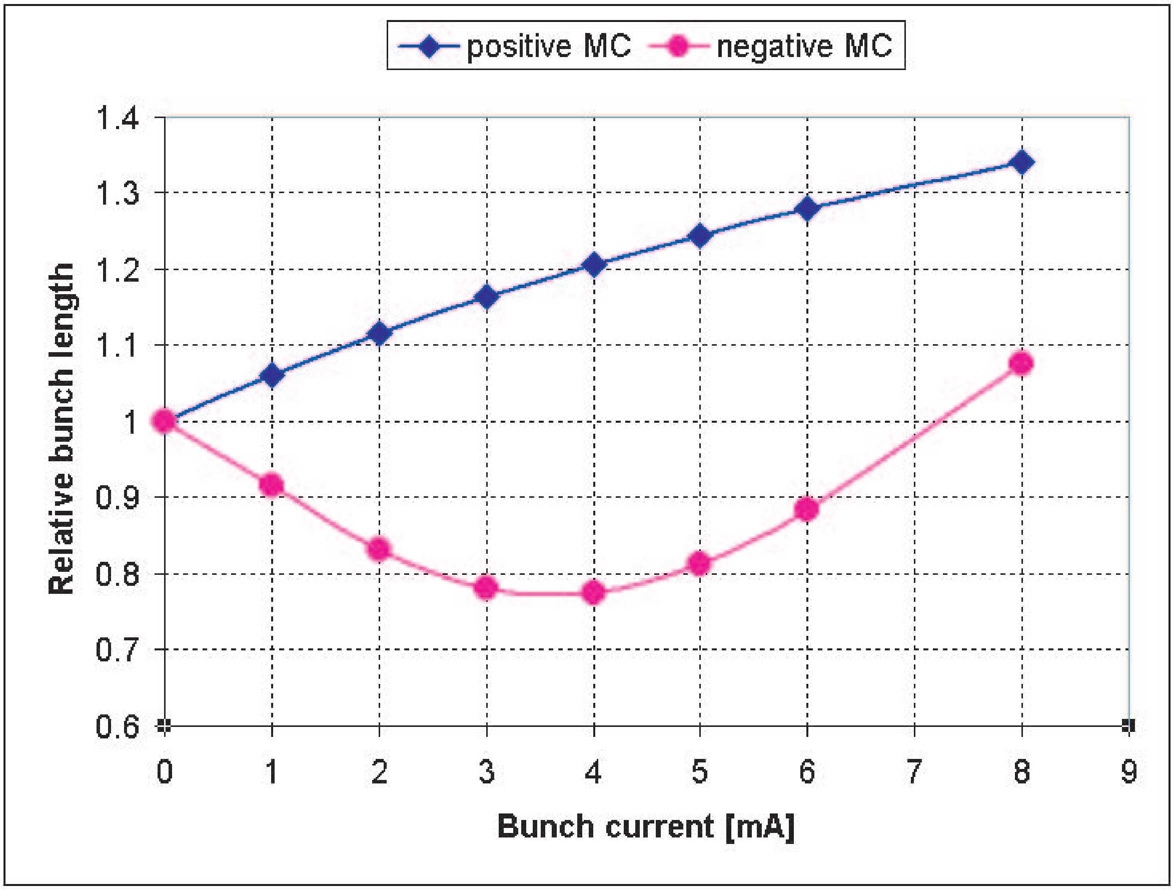

Figure 7: Bunch lengthening vs bunch current for positive and negative momentum compaction (MC) factors.

9 Beam loading

The rf beam loading in the case of two bunches per rf bucket is different from the nominal case. As usual, the cavity with the frequency of the fundamental mode ω_c generates impedance at the rf frequency $Z_c = R_L \cos(\psi) e^{i\psi}$ where $R_L = R_0/(1+\beta)$ is loaded shunt impedance, ψ is detuning angle, $\tan(\psi) = Q_L(\omega_{rf}/\omega_c - \omega_c/\omega_{rf})$, and β is the rf coupling coefficient. The rf voltage is

$$V_{cav} = (1/2)\left(V_c e^{-i\omega_{rf}t} + c.c\right) = |V_c| \cos(\omega_{rf}t - \phi_c), \tag{13}$$

where the amplitude $V_c = |V_{cav}|e^{-i\phi_c}$ and ϕ_c is the beam angle in respect to the generator current. We define the generator current I_g with the zero phase and denote the amplitudes of the beam currents of both bunches by

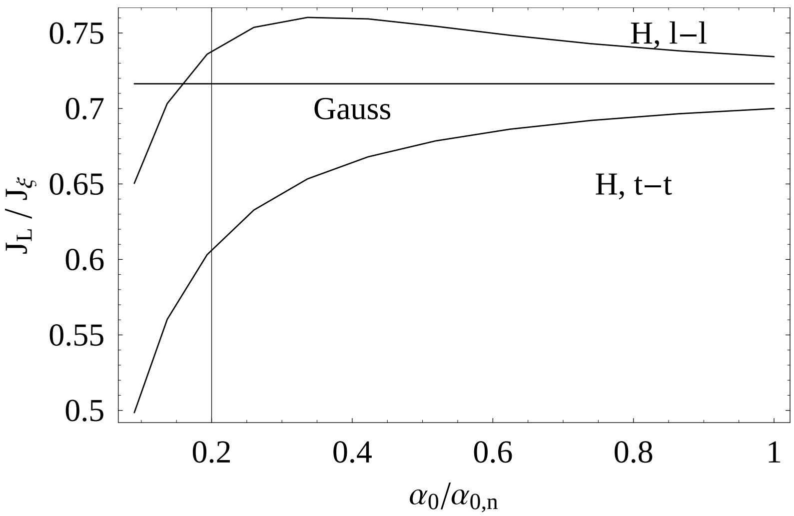

Figure 8: The ratio of the form factors J_L/J_ξ vs momentum compaction factor α_0 for β_y^* scaled as $\beta_y^* = \beta_{y,0}^*\sqrt{\alpha_0/\alpha_{0,n}}$. Parameters $\sigma_0 = \beta_{y,0}^* = 1$ cm, $\alpha_{0,n} = 2.3\,10^{-3}$, $\delta_0 = 6.1\,10^{-3}$, and the bunch current $I_b = 2.5$ mA are the nominal parameters for HER PEP-II. Three curves corresponds to the colliding Gaussian bunches, and PWD distorted (Haissinski) bunches: (H, l-l) for two leading (l) bunches and (H,t-t) for two trailing (t) bunches.

$$I_1 = I_{b1}e^{i(\phi_s-\phi_c+\xi_1)}, \quad I_2 = I_{b2}e^{i(-\phi_s-\phi_c-\xi_2)}, \tag{14}$$

where ϕ_s is the steady-state rf phase, I_{b1} and I_{b2} are real, and $\xi_{1,2}$ are small phase deviation from the steady-state due to synchrotron oscillations,

$$\xi_1 = -\frac{\omega_{rf}z_1}{c}, \quad \xi_2 = \frac{\omega_{rf}z_2}{c}. \tag{15}$$

The beam amplitudes are given by the dc currents of both beams, $I_{b1} = 2I_1^{dc}$, $I_{b2} = 2I_2^{dc}$.

The amplitudes are related by the equation

$$V_c = Z_c(I_g - I_1 - I_2) \tag{16}$$

what is equivalent to the following two equations for real quantities:

$$\begin{aligned} I_g\sin(\psi+\phi_c) &= I_{b1}\sin(\psi+\phi_s+\xi_1) + I_{b2}\sin(\psi-\phi_s-\xi_2), \\ |V_c| &= R_L\cos\psi[I_g\cos(\psi+\phi_c) - I_{b1}\cos(\psi+\phi_s+\xi_1) - I_{b2}\cos(\psi-\phi_s-\xi_2)]. \end{aligned} \tag{17}$$

Accelerating voltage for each beam is $V_{ac} = |V_c|\cos(\phi_s+\xi_{1,2})$. Because $dz_{1,2}/dt = \mp\alpha_0\delta c$, the variation $\xi_{1,2} > 0$ for the energy variation $\delta > 0$ provided $\alpha_0 > 0$. Therefore, the Robinson condition of stability for $\alpha_0 > 0$ requires

$$[dV_{ac}/d\xi_{1,2}]_{\xi=0} < 0. \tag{18}$$

The quantities I_g, ψ, ϕ_s and I_{b1}, I_{b2} should be considered as constants independent of $\xi_{1,2}$ and derivatives $d\phi_c/d\xi_{1,2}$ can be obtained from the first of Eq. 17,

$$\frac{d\phi_c}{d\xi_{1,2}} = \pm\frac{I_{b1,b2}}{I_g}\frac{\cos(\phi_s + \xi_{1,2} \pm \psi)}{\cos(\psi + \phi_c)}. \tag{19}$$

The optimum condition corresponds to the zero reflected power. That gives conditions $\phi_c = 0$ and $|V_c| = I_g R_0/(2\beta$. Excluding I_g we get

$$\begin{aligned} \beta &= \frac{\sin(\phi_s + \psi) - \kappa\sin(\phi_s - \psi)}{\sin(\phi_s + \psi) - \kappa\sin(\phi_s - \psi)}, \\ 1 &= \frac{Y}{2\sin\psi}[\sin(\phi_s - \psi) - \kappa\sin(\phi_s + \psi)], \end{aligned} \tag{20}$$

where we used parameters

$$\kappa = \frac{I_{b2}}{I_{b1}}, \quad Y = \frac{R_0 I_{b1}}{|V_c|}. \tag{21}$$

Eq. 20 can be written in the form

$$\begin{aligned} &\beta = 1 + Y(1+\kappa)\cos\phi_s \\ &\frac{\tan(\phi_s)}{\tan(\psi)} = (\frac{1+\kappa}{1-\kappa})(\frac{\beta+1}{\beta-1}). \end{aligned} \tag{22}$$

Eq. 22 defines the optimum tuning angle ψ. In the case $\kappa = 0$ and Eq. 22 give the usual expressions for a single beam.

The conditions of stability Eq. 18 in the optimum $\phi_c = \xi_1 = \xi_2 = 0$ take the form

$$1 - (1-\kappa)\frac{\tan\phi_s}{\tan\psi} < 0, \quad \kappa - (1-\kappa)\frac{\tan\phi_s}{\tan\psi} < 0. \tag{23}$$

Using Eq. 22 that can be written as $2 + (1+\beta)\kappa > 0$ and $2\kappa + 1 + \beta > 0$, what is always true. Therefore, the beam is stable.

In the limit of equal currents, $\kappa- > 1$, and the detuning angle goes to zero,

$$\psi = (\frac{Y\sin\phi_s}{2(1+Y\cos\phi_s)})(1-\kappa). \tag{24}$$

For equal beam currents there is no need to detune the cavities. That can simplify the longitudinal feedback system.

10 Microwave Instability

Sometimes, the main objection to the lattice with small momentum compaction α_0 is based on expectation of the substantially reduced threshold of the microwave instability.

Dependence of the energy spread is shown in Fig. (9) for positive and negative momentum compaction (MC) factors for the same wake. The result is obtained with the code [3] developed by one of the authors (S. N.) The threshold of instability I_{th} is indicated by the growth of the energy spread for the bunch current $I > I_{th}$.

As the figure shows, the $\propto$ 20 mA threshold for $\alpha_0 >$) is reduced to 5 mA for $\alpha_0 < 0$. However, even 5 mA bunch current is by a factor two higher that the present PEP-II bunch current and may be acceptable.

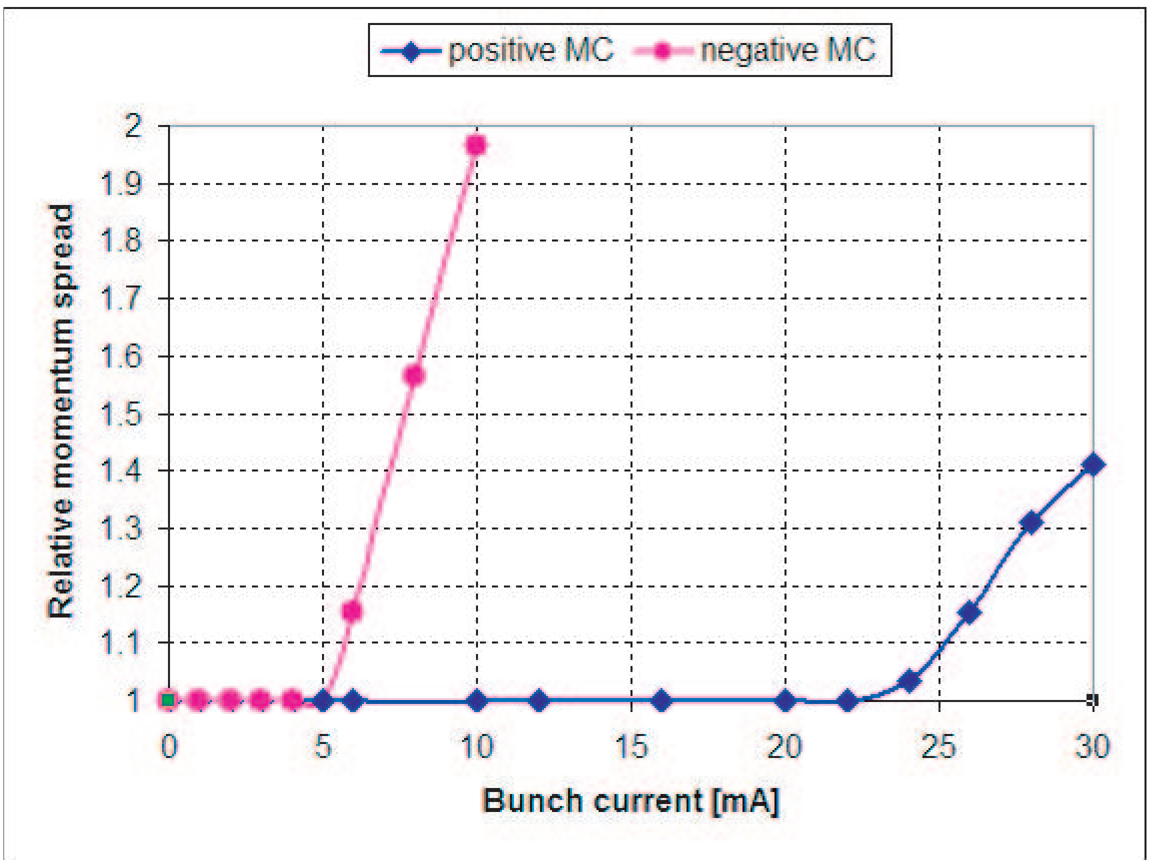

Figure 9: Energy spread vs beam current for positive and negative momentum compaction factors.

11 Longitudinal head-tail instability

The longitudinal head-tail instability is, probably, the main problem of the low-momentum compaction lattices. The growth rate of instability [1] $1/\tau \propto (\alpha_1/\alpha_0)$. For the case of $\alpha_1 \simeq \alpha_0$ the growth rate is low and the instability is usually suppressed by the synchrotron radiation (SR) damping. The situation is different for our case with the large ratio (α_1/α_0). The growth rate in this case may exceed the SR damping. An example of the strong instability for the 2 mA bunch is shown in Fig. (10).

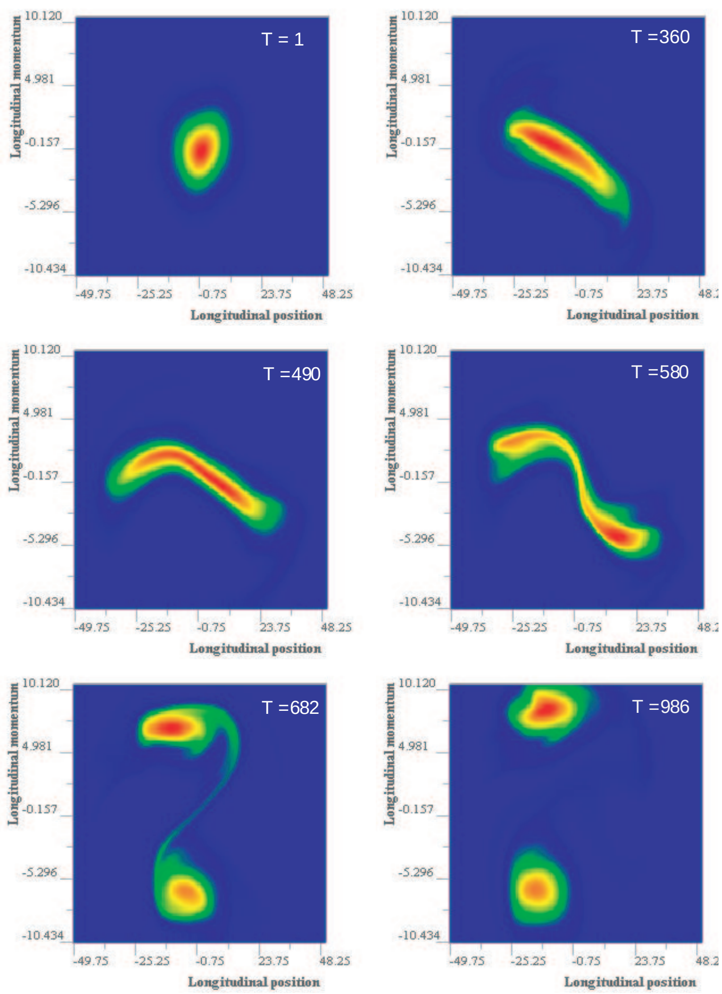

Figure 10: Dynamics of the head-tail single-bunch instability is shown in the phase plane (z, δ) for 2 mA bunch current. Time is indicated in the figure. At $t > 600$ turns, the bunch splits in halves. Results are calculated using the direct solution of the Fokker-Plank equation [3].

We carried out two type of simulations. In the simple simulations, we calculate trajectories of four particles solving with MATHEMATICA equations of motion which include synchrotron oscillations and interaction between particles proportional to the wake convoluted with $\sigma = 8$ mm Gaussian bunch,

$$\frac{d\zeta_i}{d\tau} = -\delta_i(1 + \epsilon\delta_i), \tag{25}$$
$$\frac{d\delta_i}{d\tau} = \zeta_i - \sum_j I_{\frac{bunch}{4}} W[\zeta_i - \zeta_j,$$

where $(i, j) = 1, 2, ..., 4$, the dimensionless ζ is the distance of a particle from the bunch center in units of the rms bunch σ and δ is relative energy offset $\Delta E/E$ in units of the relative rms energy spread δ_0, $\tau = \omega_s t$, and $\epsilon = (\alpha_1/\alpha_0)\delta_0$. Note that in this units one revolution period $T_0 = 2\pi$. In the simulations we used LER parameters, the synchrotron period equal to 56 revolution periods, $\alpha_0 = 5.34\,10{-}4$, $\alpha_1 = 5.54\,10{-}4$, $\delta_0 = 7.7\,10^{-4}$, and $\sigma = 8$ mm. Trajectories with initial conditions $\zeta_i = -0.33, -0.27, 0.27, 0.33$, $\delta_i = 0$, were calculated for the time interval up to 700 synchrotron periods. That allows fast study of the dynamics of the system including quantitative result for the emittance variation. More elaborate simulations used the Fokker-Plank solver developed to study microwave instability.

Results of the simple simulations for the bunch current $I_{bunch} = 0.5$ mA are shown in Fig. (11).

The system in clearly unstable although the growth rate is small. However, the instability is peculiar one: although it is the single bunch instability, the mechanism of instability is related to the nonlinear motion of the bunch centroid. More precisely [1], the instability is caused by the variation of the energy loss during the synchrotron period due to variation of the rms bunch length. Therefore, it seems that the instability might be stabilized by the longitudinal feedback system (FB). We model the FB generating a buffer $\zeta_1, ..., \zeta_{56}$ with positions of the bunch centroid for each of 56 revolutions per synchrotron period. The buffer is redefined each turn to keep data on the last 56 turns and the data are interpolated as the sum of

$$\zeta_f(\tau_k) = a_0 + a_1 \sin(\nu\tau_k + \phi_1) + a_2 \sin(2\nu\tau_k + \phi_2) + a_3 \sin(3\nu\tau_k + \phi_3), \tag{26}$$

where $\tau_k = \tau - (k-1)T_0$, $k = 1, ..., 56$, and a_j, $j = 0, 1, 2, 3$ and ϕ_j, $j = 1, 2, 3$ are fitting parameters. The buffer is redefined each turn to keep data on the last 56 turns.. Then, the same kick $\delta_i \to \delta_i + K$ is applied to each of four tracking particles where $K = 0.1\, d\zeta_f(\tau/d\tau)$ is proportional to the derivative of the fitting function taken at $k = 1$. The coefficient 0.1 was determined to give the best damping. The result of tracking for each of the particles with the FB on is shown in Fig. (12). The results seems encouraging: the amplitude of the oscillations for each particle remain stable for 700 synchrotron periods.

Unfortunately, the simulations with the Fokker-Plank solver do not confirm this conclusion, see Fig. (13) and Fig. (14). Although the results in many respect seems similar to the four-particle model, there is a systematic growth of the bunch emittance in spite of the feedback included in the simulations in the same way as it is described above. The difference of two simulations is apparently due to the difference in the models: the two-particle model does not include fluctuations which are included in the Fokker-Plank equation.

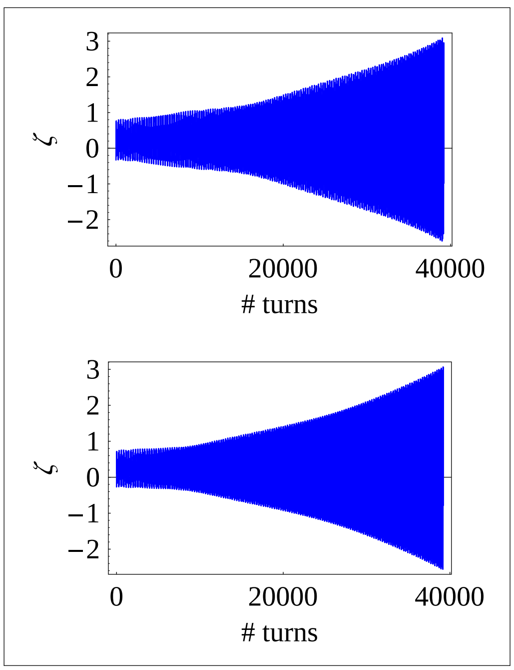

Figure 11: Tracking of four particles with the feedback off, $I_{bunch} = 0.5$ mA. The trajectories are unstable.

12 Summary

The quasi-isochronous ring with the reduced momentum compaction factor allows to have two stable bunches per rf bucket. It is tempting to increase the number of bunches per ring without increasing the rf frequency. The paper presents a preliminary study of this possibility. We consider the lattice design, the bunch lengthening and distortion, parasitic

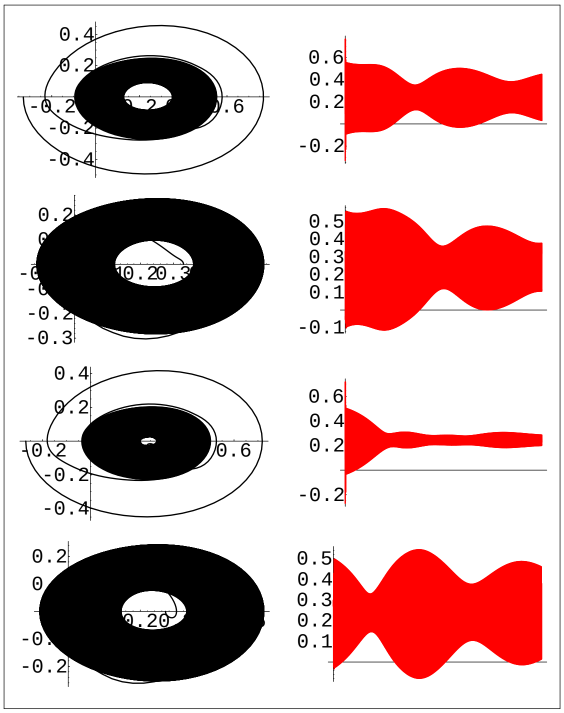

Figure 12: Tracking of four particles with the feedback on. The i-th row shows the trajectory in the phase plane (on the left) and time variation $\zeta_i(\tau)$ (on the right) for the $i = 1, 2, 3, 4$ particle. The trajectory after one or two turns finds the fix point and then remains stable for 700 synchrotron periods.

crossings, the rf beam stability, microwave and longitudinal head-tail instabilities. The problem of the higher rf power remains and is similar to that for the filling of each rf bucket. Additional parasitic crossing affects the luminosity but the adverse effect may be less than the gain in luminosity due to additional bunches. The bunch lengthening and microwave instability seems to give week constraints. However, the longitudinal head-tail instability makes the beam unstable and the feeback system can not stabilize it although the growth rate of instability is small. Therefore, the statement that there are two stable fix points in the low alpha lattices is an illusion: the fluctuations make the particles in the second fixed point unstable.

The authors thank Y. Nosochkov for his help with MAD.

References

[1] Handbook of Accelerator Physics and Engineering, Edited by A. W. Chao and M. Tigner, World Scientific

[2] W. J. Corbett, M. H.R. Donald, A.A. Garren, An isochronous lattice for PEP, SLAC-PUB-5538, LBL-30669, April 1991. Presented at The IEEE PAC, SF, CA, May 6-9 1991.

[3] A. Novokhatski, "Computer Algorithm for Longitudinal Single Bunch Stability Study in a Storage Ring", SLAC-PUB-11251, May, 2005

13 Appendix: Quasi-isochronous supercell

```
THETA := 0.0218166, par1=-7.334216, par2=-4.810802
   HB: SBEND, L=2.7, ANGLE=THETA, E1=0.5*THETA, E2=0.5*THETA
   QF1: QUAD, L=0.25, K1=0.49
   QD1: QUAD, L=0.25, K1=-0.2257767
   QF2: QUAD, L=0.25, K1= 0.3020760
   QD2: QUAD, L=0.25, K1= -0.2470620
   SF1: SEXTUPOLE, L=0.25, K2=par1
   SD1: SEXTUPOLE, L=0.25, K2=par2
   D1: DRIFT, L=0.85
   D2: DRIFT, L=1.0
   D3: DRIFT, L=0.60
   HCEL1: LINE=(QF1,D1,HB,HB,D3,SF1,QD1)
   HCEL2: LINE=(QF2,D1,HB,HB,D3,SF1,QD1)
   HCEL3: LINE=(QF2,D1,HB,HB,D3,SD1,QD2)
   CEL1: LINE=(HCEL1,-HCEL2)
   CEL2: LINE=(HCEL3,-HCEL3)
   CEL3: LINE=(HCEL2,-HCEL1)
   SuperCell: LINE=(CEL1,CEL2,CEL3)
```

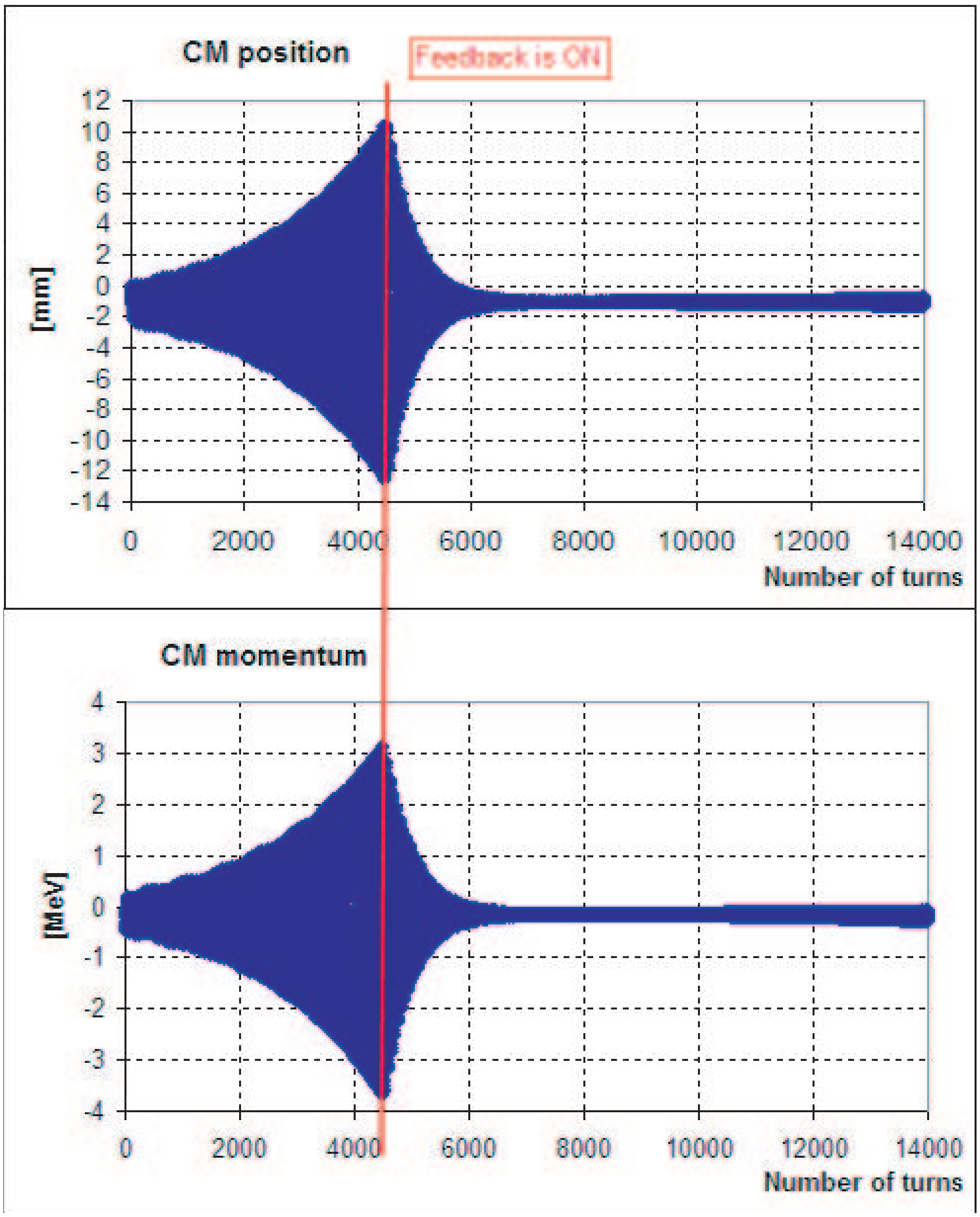

Figure 13: Variation of the centroid offset and the centroid energy in time with zero wake. Results are from the solution of the Fokker-Plank equation with the feedback on.

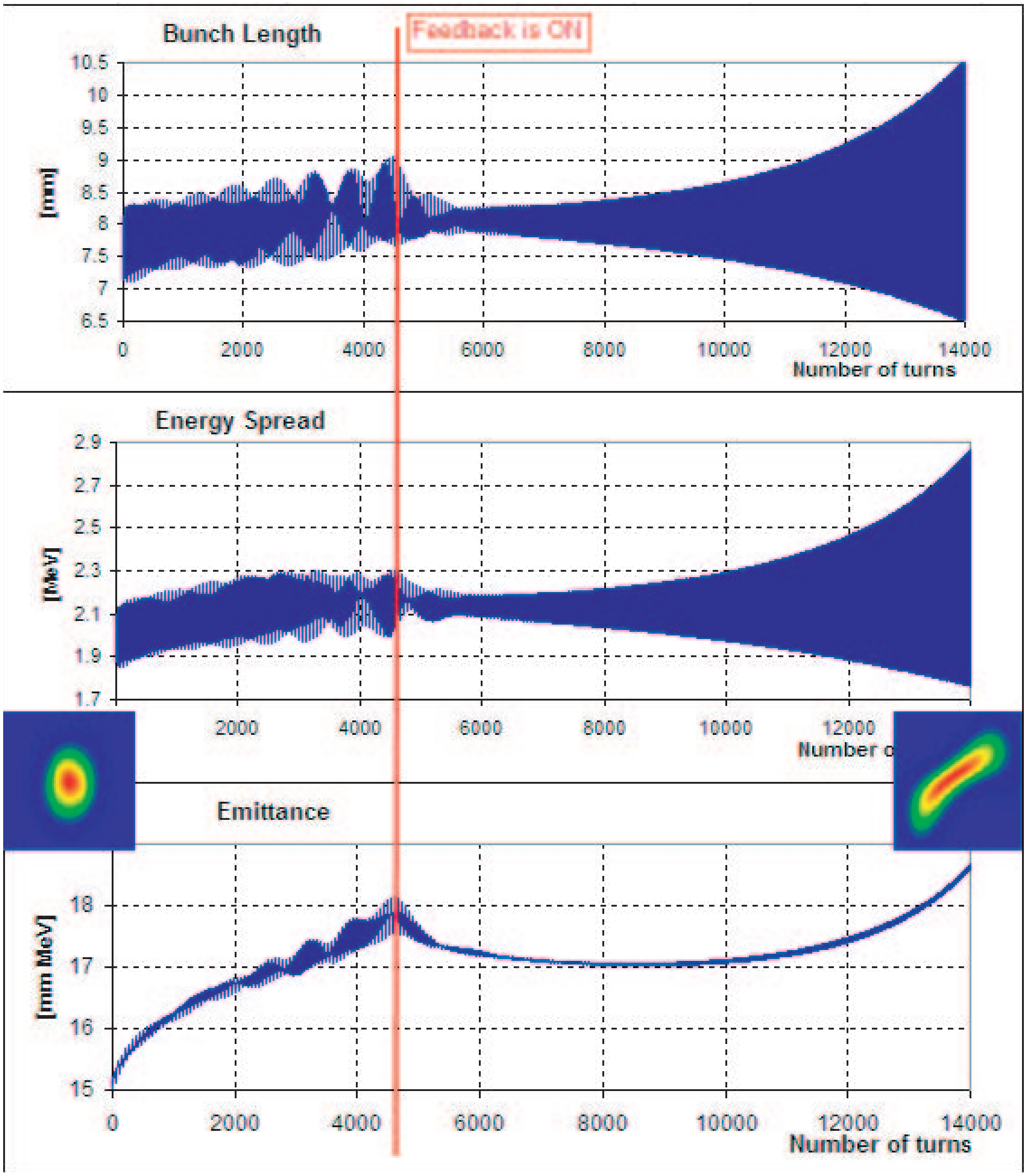

Figure 14: Variation of the bunch length, the energy spread, and emittance in time. Results are from the solution of the Fokker-Plank equation with the feedback on. The fast growth starts with the bunch deformation (see insert) which is later would followed by splitting of thge bunch in halves as shown in Fig. (10).